

## Stereoselective Assembly of Gigantic Chiral Molybdenum Blue Wheels Using Lanthanide Ions and Amino Acids

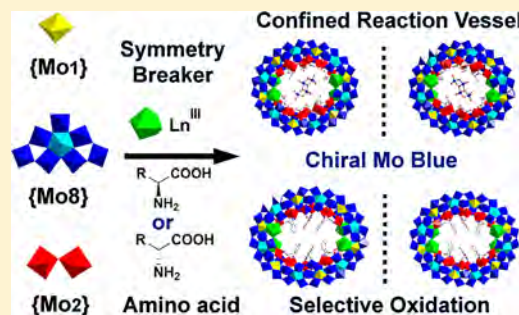
Weimin Xuan, Robert Pow, Nancy Watfa, Qi Zheng, Andrew J. Surman, De-Liang Long,<sup>†</sup> and Leroy Cronin<sup>\*†</sup>

WestCHEM, School of Chemistry, The University of Glasgow, Glasgow G12 8QQ, United Kingdom

### Supporting Information

**ABSTRACT:** The synthesis of chiral polyoxometalates (POMs) is a challenge because of the difficulty to induce the formation of intrinsically chiral metal-oxo frameworks. Herein we report the stereoselective synthesis of a series of gigantic chiral Mo Blue (MB) POM clusters 1–5 that are formed by exploiting the synergy between coordinating lanthanides ions as symmetry breakers to produce MBs with chiral frameworks decorated with amino acids ligands; these promote the selective formation of enantiopure MBs. All the compounds share the same framework archetype, based on  $\{\text{Mo}_{124}\text{Ce}_4\}$ , which forms an intrinsically chiral  $\Delta$  or  $\Lambda$  configurations, controlled by the configurations of functionalized chiral amino acids. The chirality and stability of 1–5 in solution are confirmed by circular dichroism,  $^1\text{H}$  NMR, and electrospray ion mobility–mass spectrometry studies.

In addition, the framework of the  $\{\text{Mo}_{124}\text{Ce}_4\}$  MB not only behaves as a host able to trap a chiral  $\{\text{Mo}_8\}$  cluster that is not accessible by traditional synthesis but also promotes the transformation of tryptophan to kynurenine *in situ*. This work demonstrates the potential and applicability of our synthetic strategy to produce gigantic chiral POM clusters capable of host–guest chemistry and selective synthetic transformations.



### INTRODUCTION

Polyoxometalates (POMs) are a unique class of discrete metal oxides with a diversity of structures and properties.<sup>1,2</sup> As such, POMs have a wide range of potential applications from medicine to catalysis and materials science.<sup>3</sup> One focus of POM chemistry is the controlled fabrication of chiral POM clusters that are potential candidates in asymmetric catalysis, chiral separations, sensors and biomedicine.<sup>4</sup> During the past two decades, a variety of chiral POM clusters have been designed and synthesized via either chiral resolution and spontaneous resolution of the intrinsically chiral POMs or stereoselective synthesis driven by chirality transfer from chiral organic ligands or metal–organic species.<sup>5</sup> Despite the synthesis of chiral gigantic POMs, the assembly of systems with chiral frameworks has proved challenging. This is due to their very high symmetries and large skeletons composed of hundreds of metal and oxygen atoms; together, these make it hard to form intrinsically chiral POMs or achieve chirality transfer. Moreover, the chiral functionalization of wheel- or cage-shaped gigantic POMs is particularly interesting, not only because they could provide confined chiral environments for asymmetric processes such as asymmetric catalysis and chiral recognition but also because they could be potentially used as model compounds as “artificial proteins” to mimic functional biological systems.<sup>6</sup> To the best of our knowledge, there have been no reports of chiral POMs with nuclearity of >100.

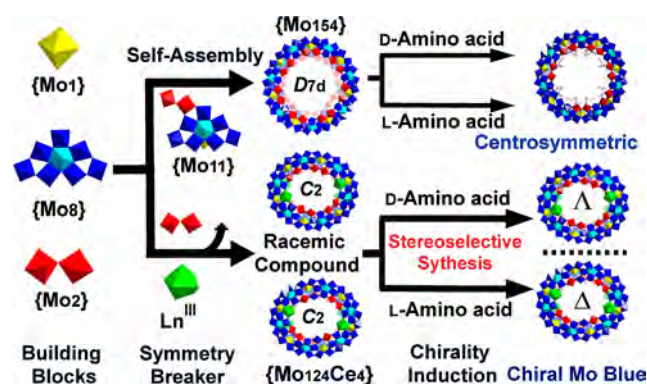
Molybdenum blue (MB) compounds are a family of gigantic isopolyoxomolybdates clusters, including the archetype

wheel-shaped  $\{\text{Mo}_{154}\}$  and  $\{\text{Mo}_{176}\}$  and lemon-shaped  $\{\text{Mo}_{368}\}$  that are constructed from basic  $\{\text{Mo}_8\}$ ,  $\{\text{Mo}_2\}$ , and  $\{\text{Mo}_1\}$  building blocks.<sup>7</sup> The  $\{\text{Mo}_2\}$  units are the reactive sites and could be easily coordinated by amino acid ligands (AA) or replaced by electrophiles such as lanthanides.<sup>8,9</sup> Indeed, cystine and tyrosine have been successfully grafted onto the archetypal  $\{\text{Mo}_{154}\}$ .<sup>9</sup> Nevertheless, none of these AA-functionalized  $\{\text{Mo}_{154}\}$  clusters exhibit chirality in the solid-state, and they crystallize in centrosymmetric space groups (Scheme 1). In contrast, elliptical lanthanide-doped MB (LMB) such as dimeric  $\{\text{Mo}_{256}\text{Eu}_8\}$ ,  $\{\text{Mo}_{120}\text{Pr}_6\}$ , and  $\{\text{Mo}_{100}\text{Ce}_6\}$  can be produced by substitution of the  $\{\text{Mo}_2\}$  groups by smaller lanthanide ions. The incorporation of lanthanide ions “breaks” the  $D_{7d}$  symmetry of parent  $\{\text{Mo}_{154}\}$  on reorganization and yields clusters with much lower molecular symmetries, for example,  $C_1$  for  $\{\text{Mo}_{256}\text{Eu}_8\}$ ,<sup>8a</sup>  $D_3$  for  $\{\text{Mo}_{120}\text{Pr}_6\}$ ,<sup>8b</sup> and  $C_2$  for  $\{\text{Mo}_{100}\text{Ce}_6\}$ .<sup>8c</sup> This means the molecular structures of single wheels of these LMB are essentially chiral; however, the opposite enantiomers are always present in an equivalent amount due to the presence of either an inversion center, or mirror plane and thus makes the arrangements racemic. We hypothesized that the combination of lanthanides as “symmetry breakers” and amino acids as chiral ligands may exert a synergistic effect that could facilitate the stereoselective synthesis of chiral MBs (Scheme 1). As shown in Scheme 1, racemic LMBs consist of

Received: September 8, 2018

Published: November 29, 2018

**Scheme 1. Schematic of the Stereoselective Synthesis of Chiral MB by Using Lanthanides as “Symmetry Breaker” and Amino Acids as Chiral Ligands<sup>a</sup>**



<sup>a</sup>See Figure 1 for more details regarding  $\Delta$  and  $\Lambda$  configurations of chiral Mo Blue.

two opposite enantiomers and form in the first step by employing lanthanide ions as a “symmetry breaker”. In the presence of either D- or L- amino acids, the single enantiomer of chiral LMB could be formed by the stereoselective synthesis of chiral structures due to the chirality transfer/induction from chiral ligands in the second step. The enantiomers can be discriminated using  $\Delta$  and  $\Lambda$  nomenclature for the individual isomers. In coordination chemistry, the absolute configuration of chiral compounds adopting right-handed helical arrangement is designated as  $\Delta$ , while  $\Lambda$  is used for left-handed helical arrangement (Scheme 1).

Herein we report the stereoselective synthesis of a series of chiral MB  $\Delta$ -1 and  $\Lambda$ -1, 2, 3,  $\Delta$ -4 and  $\Lambda$ -4,  $\Delta$ -5 and  $\Lambda$ -5 by using  $\text{Ce}^{3+}$  ions as symmetry breakers, and amino acids as chiral ligands to confirm our hypothesis. In contrast, compounds 6 and 7, synthesized under similar conditions but without addition of  $\text{Ce}^{3+}$  ions, crystallize in centrosymmetric space groups. All compounds were characterized crystallographically and the formulations are fully supported using extensive analytical techniques (see the Supporting Information).

## RESULTS AND DISCUSSION

**Synthesis of 1–7.** Compounds  $\Delta$ -1 and  $\Lambda$ -1 were synthesized from a one-pot reaction of  $\text{Na}_2\text{MoO}_4 \cdot 2\text{H}_2\text{O}$ ,  $\text{CeCl}_3 \cdot 7\text{H}_2\text{O}$ ,  $[\text{N}_2\text{H}_4] \cdot 2\text{HCl}$  and L-/D-histidine at 90 °C. Heating is essential for the formation of chiral wheels as the reaction mixture was turbid when mixing all the starting materials at r.t. Upon heating, the solution turned to a clear, deep-blue solution in 10–15 min. The concentration of the amino acid reagents in the reaction mixture is also critical. Higher concentrations were found to promote crystal growth quickly, and thus result in a crystalline solid with poor crystallinity, while lower concentrations lead to good crystals but with a longer crystallization time and lower yields. Adopting the same procedure as  $\Lambda$ -1 but slightly decreasing the amount of L-histidine produced compound 2, while compound 3 was discovered during the scale-up synthesis of  $\Lambda$ -1. Overall, the reactions are controlled by adjustment of the amount of L-histidine. A slight reduction of L-histidine will slow down the crystallization and initiate the formation of isomeric 2 and 3 instead of  $\Delta$ -1. Inspired by the successful synthesis of 1–3, more amino acids have been explored, and compounds 4 and 5 were synthesized using arginine and tryptophan, respectively.

We have also tried other amino acids such as alanine and phenylalanine; however, either precipitate or very small crystals were obtained. 6 and 7 were synthesized in a straightforward way, without addition of  $\text{CeCl}_3 \cdot 7\text{H}_2\text{O}$  to afford, respectively, L-histidine- and L-tryptophan-functionalized  $\{\text{Mo}_{154}\}$  in good yield and high purity. This shows that the use of the lanthanide ions is critical in restructuring the MB wheel.

**Determination of the Formulas of 1–7.** The determination of the formulas of the Mo-blues has been well established and requires a series of analytical techniques including redox titrations, UV–vis–NIR spectroscopy, bond valence sum analysis (BVS), elemental analysis, and thermogravimetric analysis (TGA), in addition to single-crystal X-ray diffraction analysis (see the Supporting Information for details).<sup>11</sup> Herein,  $\Lambda$ -1 was selected to exemplify the general approach used to determine the formula. First, BVS calculations were carried out on all the Mo and O centers, revealing that  $\Lambda$ -1a is composed of a 24-electron reduced anionic ring containing 12 singly and 60 doubly protonated oxygen atoms.<sup>12</sup> Singly protonated are the 12 equivalent oxo atoms situated in the equatorial plane and linking two neighboring  $\{\text{Mo}_8\}$  units as well as  $\{\text{Mo}_1\}$  units. BVS could not be applied to highly distorted  $\{\text{Mo}_8\}$  due to the disorder of these groups. Therefore, all the Mo centers on  $\{\text{Mo}_8\}$  are assumed to be  $\text{Mo}^{\text{VI}}$ , consistent with previous work.<sup>8</sup> Meanwhile, redox titration and UV–vis–NIR spectroscopy could not be used to determine the overall reduction state for  $\Lambda$ -1a because of its very poor solubility. However, elemental analysis confirms the framework of 1a consists of 124 Mo and 4 Ce atoms, consistent with the structural refinement done using the single-crystal X-ray diffraction data. Taking into consideration the information obtained from the calculations above, along with elemental analysis, it is possible to determine the overall building-block scheme and overall charge for  $\Lambda$ -1a as  $[\{\text{Mo}_8\}_{26}\{\{\text{Mo}_2\}_8\{\text{Mo}_1\}_{12}\{\text{Mo}_8\}_{12}\{\text{Ce}(\text{H}_2\text{O})_5\}_4\}]^{12-} \equiv \{\text{Mo}^{\text{VI}}_8\text{O}_{26}\}[\{\text{Mo}^{\text{VI}}_2\text{O}_5(\text{H}_2\text{O})_2\}_8\{\text{Mo}^{\text{VI/V}}_8\text{O}_{26}(\mu\text{-O})_2\text{H}(\text{H}_2\text{O})_3\text{Mo}^{\text{VI/V}}\}_{12}\{\text{Ce}^{\text{III}}(\text{H}_2\text{O})_5\}_4\{\text{C}_6\text{H}_9\text{N}_3\text{O}_2\}_6]^{12-}$ . Second, to balance the negative charge of  $-12$ , 10 protons and 2 protonated L-histidines are proposed as counterions as the content of Na is negligible as found in the elemental analysis data (0.026%). The amount of L-histidine was deduced from C, H, and N analysis, and a total eight L-histidines are found in the structure of  $\Lambda$ -1. Among them, six are located on the framework of  $\Lambda$ -1a while another two are counterions. Finally, the TGA curve of  $\Lambda$ -1 exhibits a total weight loss of 11.6% from r.t. to 150 °C, which corresponds to  $\sim 165$  guest water molecules. On the basis of what discussed above, the formula of  $\Lambda$ -1 could therefore be determined as  $\text{H}_{10}(\text{C}_6\text{H}_{10}\text{N}_3\text{O}_2)_2\{\{\text{Mo}_8\}_{26}\text{Mo}_{124}\text{Ce}_4\text{O}_{376}(\text{H}_2\text{O})_{60}\text{H}_{12}(\text{C}_6\text{H}_9\text{N}_3\text{O}_2)_6\} \cdot 165\text{H}_2\text{O} \equiv \text{H}_{10}(\text{C}_6\text{H}_{10}\text{N}_3\text{O}_2)_2\{\Lambda\text{-1a}\} \cdot 165\text{H}_2\text{O}$ . The formulas of compounds 2–7 are determined in a similar manner. Compounds 1–7 could be formulated as follows:

- $\Lambda$ -1:  $\text{H}_{10}(\text{C}_6\text{H}_{10}\text{N}_3\text{O}_2)_2\{\{\text{Mo}_8\}_{26}\text{Mo}_{124}\text{Ce}_4\text{O}_{376}(\text{H}_2\text{O})_{60}\text{H}_{12}(\text{C}_6\text{H}_9\text{N}_3\text{O}_2)_6\} \cdot 165\text{H}_2\text{O} \equiv \text{H}_{10}(\text{C}_6\text{H}_{10}\text{N}_3\text{O}_2)_2\{\Lambda\text{-1a}\} \cdot 165\text{H}_2\text{O}$
- $\Delta$ -1:  $\text{H}_{10}(\text{C}_6\text{H}_{10}\text{N}_3\text{O}_2)_2\{\{\text{Mo}_8\}_{26}\text{Mo}_{124}\text{Ce}_4\text{O}_{376}(\text{H}_2\text{O})_{60}\text{H}_{12}(\text{C}_6\text{H}_9\text{N}_3\text{O}_2)_6\} \cdot 165\text{H}_2\text{O} \equiv \text{H}_{10}(\text{C}_6\text{H}_{10}\text{N}_3\text{O}_2)_2\{\Delta\text{-1a}\} \cdot 165\text{H}_2\text{O}$
- 2:  $\text{Na}_3\text{H}_5(\text{C}_6\text{H}_{10}\text{N}_3\text{O}_2)_2\{\{\text{Mo}_{124}\text{Ce}_4\text{O}_{376}(\text{H}_2\text{O})_{64}\text{H}_{12}(\text{C}_6\text{H}_9\text{N}_3\text{O}_2)_4\}_{0.5}\{\{\text{Mo}_8\}_{26}\text{Mo}_{124}\text{Ce}_4\text{O}_{376}(\text{H}_2\text{O})_{60}\text{H}_{12}(\text{C}_6\text{H}_{10}\text{N}_3\text{O}_2)_6\}_{0.5}\} \cdot 170\text{H}_2\text{O} \equiv \text{Na}_3\text{H}_5(\text{C}_6\text{H}_{10}\text{N}_3\text{O}_2)_2\{\mathbf{2a}_1\}_{0.5}\{\mathbf{2a}_2\}_{0.5} \cdot 170\text{H}_2\text{O}$



- 3:  $\text{H}_{12}\{\text{Mo}_8\text{O}_{26}\}\text{Mo}_{124}\text{Ce}_4\text{O}_{376}(\text{H}_2\text{O})_{60}\text{H}_{12}(\text{C}_6\text{H}_9\text{N}_3\text{O}_2)_6 \cdot 155\text{H}_2\text{O} \equiv \text{H}_{12}\{3\mathbf{a}\} \cdot 155\text{H}_2\text{O}$
- $\Delta$ -4:  $\text{Na}_2\text{H}_4(\text{C}_{10}\text{H}_{13}\text{N}_2\text{O}_3)_2\{\text{Mo}_{124}\text{Ce}_4\text{O}_{376}(\text{H}_2\text{O})_{60}\text{H}_{12}(\text{C}_{11}\text{H}_{12}\text{N}_2\text{O}_2)_6\} \cdot 150\text{H}_2\text{O} \equiv \text{Na}_2\text{H}_4(\text{C}_{10}\text{H}_{13}\text{N}_2\text{O}_3)\{\Delta\text{-}4\mathbf{a}\} \cdot 150\text{H}_2\text{O}$
- $\Lambda$ -4:  $\text{Na}_2\text{H}_4(\text{C}_{10}\text{H}_{13}\text{N}_2\text{O}_3)_2\{\text{Mo}_{124}\text{Ce}_4\text{O}_{376}(\text{H}_2\text{O})_{60}\text{H}_{12}(\text{C}_{11}\text{H}_{12}\text{N}_2\text{O}_2)_6\} \cdot 150\text{H}_2\text{O} \equiv \text{Na}_2\text{H}_4(\text{C}_{10}\text{H}_{13}\text{N}_2\text{O}_3)\{\Lambda\text{-}4\mathbf{a}\} \cdot 150\text{H}_2\text{O}$
- $\Delta$ -5:  $\text{H}_6(\text{C}_6\text{H}_{15}\text{N}_4\text{O}_2)_2\{\text{Mo}_{124}\text{Ce}_4\text{O}_{376}(\text{H}_2\text{O})_{64}\text{H}_{12}(\text{C}_6\text{H}_{14}\text{N}_4\text{O}_2)_4\} \cdot 160\text{H}_2\text{O} \equiv \text{H}_6(\text{C}_6\text{H}_{15}\text{N}_4\text{O}_2)_2\{\Delta\text{-}5\mathbf{a}\} \cdot 160\text{H}_2\text{O}$
- $\Lambda$ -5:  $\text{H}_6(\text{C}_6\text{H}_{15}\text{N}_4\text{O}_2)_2\{\text{Mo}_{124}\text{Ce}_4\text{O}_{376}(\text{H}_2\text{O})_{64}\text{H}_{12}(\text{C}_6\text{H}_{14}\text{N}_4\text{O}_2)_4\} \cdot 160\text{H}_2\text{O} \equiv \text{H}_6(\text{C}_6\text{H}_{15}\text{N}_4\text{O}_2)_2\{\Lambda\text{-}5\mathbf{a}\} \cdot 160\text{H}_2\text{O}$
- 6:  $\text{Na}_4\text{H}_{10}\{\text{Mo}_{154}\text{O}_{462}(\text{H}_2\text{O})_{54}\text{H}_{14}(\text{C}_6\text{H}_9\text{N}_3\text{O}_2)_8\} \cdot 200\text{H}_2\text{O} \equiv \text{Na}_4\text{H}_{10}\{6\mathbf{a}\} \cdot 200\text{H}_2\text{O}$
- 7:  $\text{Na}_8\text{H}_4(\text{C}_{11}\text{H}_{13}\text{N}_2\text{O}_2)_2\{\text{Mo}_{154}\text{O}_{462}(\text{H}_2\text{O})_{54}\text{H}_{14}(\text{C}_{11}\text{H}_{12}\text{N}_2\text{O}_2)_8\} \cdot 180\text{H}_2\text{O} \equiv \text{Na}_8\text{H}_4(\text{C}_{11}\text{H}_{13}\text{N}_2\text{O}_2)_2\{7\mathbf{a}\} \cdot 180\text{H}_2\text{O}$

**Crystal Structures of 1–7.** Single-crystal X-ray structural analysis reveals that  $\Lambda$ -1 crystallizes in the chiral space group  $P2_12_12$  and features an elliptical nanoring  $\{\text{Mo}_{124}\text{Ce}_4\}$ , composed of 12  $\{\text{Mo}_8\}$  units, 8  $\{\text{Mo}_2\}$  units, 12  $\{\text{Mo}_1\}$  units, 4  $\{\text{Ce}(\text{H}_2\text{O})_3\}$  units, and 6 L-histidine, with a  $\{\text{Mo}_8\}$  cluster trapped in the center (Figure 1a,b). The four  $\text{Ce}^{3+}$  ions are distributed symmetrically on the two ends of both the upper and lower rims of  $\{\text{Mo}_{124}\text{Ce}_4\}$ , making the whole wheel exhibit an elliptical configuration with  $C_2$  symmetry. Therefore, the wheel displays a relatively symmetric structure with an oval-shaped opening with outer and inner ring diameters of about 31 and 12 Å, respectively, at its most elongated points. Adopting the definition from IUPAC,<sup>13</sup> if we draw two skew lines between two  $\text{Ce}^{3+}$  ions on the same rim, then the anticlockwise rotation of the line behind the plane relative to the line on the plane is designated as left-handed helix or vice versa. Accordingly, the absolute configuration of  $\{\text{Mo}_{124}\text{Ce}_4\}$  of  $\Lambda$ -1a is assigned as  $\Lambda$  (Figure 1c). There are six L-histidine coordinated to six  $\{\text{Mo}_2\}$  units via carboxylate groups with the side chain buried in the pitch of  $\{\text{Mo}_{124}\text{Ce}_4\}$ . Four are located on one side in two pairs, parallel with a separation between the adjacent imidazole rings of 3.884 Å, while the remaining two hang on the two ends of either side of  $\{\text{Mo}_{124}\text{Ce}_4\}$  to minimize the steric hindrance (Figure 1b). The absolute configuration of L-histidine could be unambiguously determined from spatial arrangement of the atoms around the stereogenic carbon, consistent with the chiral histidine used for synthesis (Figure 1e). Adjacent  $\Lambda$ -1a packs in parallel to the crystallographic  $ab$  plane giving rise to 1D channels occupied by protonated histidine and guest water molecules (Figure S14).

A  $\{\text{Mo}_8\}$  cluster resides in the middle of the ring with a  $C_2$  axis going through its center, anchored in place by a large number of N–H...O and C–H...O hydrogen-bonds formed with the coordinated histidine ligands grafted onto the inner ring of  $\{\text{Mo}_{124}\text{Ce}_4\}$  (Figures 1 and S13). In addition, all the histidine ligands are protonated and serve as positively charged buffers, reducing the repulsive electrostatic force between the two negatively charged species, further stabilizing the supra-molecular guest@host assembly  $\{\text{Mo}_8\}@\{\text{Mo}_{124}\text{Ce}_4\}$ . On the whole, the  $\{\text{Mo}_8\}$  cluster appears to be structurally related to the  $\gamma$ - $[\text{Mo}_8\text{O}_{26}]^{4-}$  isomer reported previously,<sup>14</sup> which is composed of 4  $\text{MoO}_6$  octahedra as central core capped by two sets of dinuclear  $\{\text{Mo}_2\}$  units consisting of one  $\text{MoO}_5$  trigonal

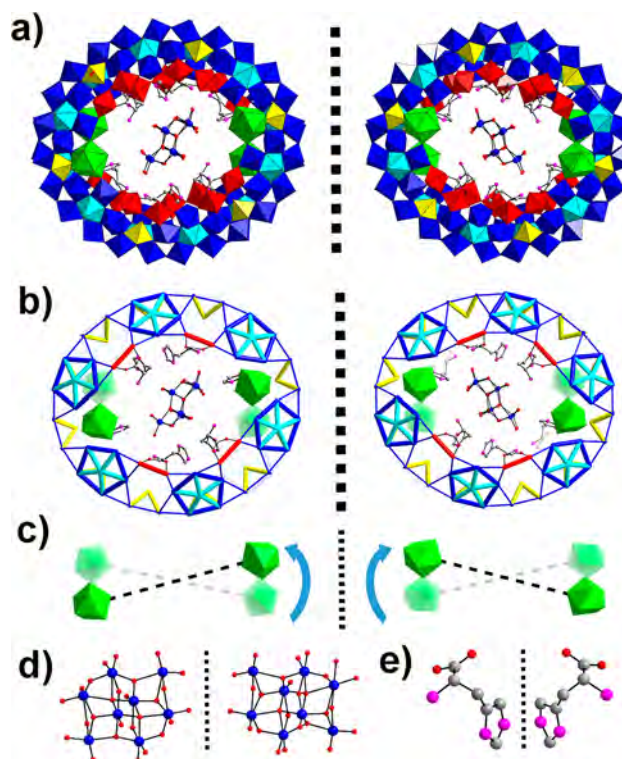


**Figure 1.** (a) View of the molecular structure of  $\Lambda$ -1 (left) and  $\Delta$ -1 (right).  $\{\text{Mo}_1\}$ , yellow polyhedron;  $\{\text{Mo}_2\}$ , red polyhedron;  $\{\text{Mo}_8\}$ , blue polyhedron with central pentagonal units in cyan polyhedron; Ce, green polyhedron; O, red; C, gray; N, pink. The entrapped  $\{\text{Mo}_8\}$  cluster and histidines are present in ball and stick model. (b) View of the simplified framework of  $\Lambda$ -1 (left) and  $\Delta$ -1 (right) to highlight the basic  $\{\text{Mo}_8\}$ ,  $\{\text{Mo}_2\}$  and  $\{\text{Mo}_1\}$  building blocks. (c) Representation of the absolute configurations of  $\Lambda$ -1 (left) and  $\Delta$ -1 (right) based on helical arrangement of  $\text{Ce}^{3+}$  ions. The  $\text{Ce}^{3+}$  ions behind the plane is highlighted in transparency. (d and e) View of the two enantiomers of entrapped  $\{\text{Mo}_8\}$  clusters and histidine in  $\Lambda$ -1 (left) and  $\Delta$ -1 (right).

bipyramid and one  $\text{MoO}_6$  octahedron. All the  $\text{MoO}_6$  octahedra and  $\text{MoO}_5$  trigonal bipyramids are linked with each other in an edge-shared mode. However, the  $\{\text{Mo}_8\}$  cluster trapped within  $\{\text{Mo}_{124}\text{Ce}_4\}$  displays a chiral configuration with a molecular symmetry of  $C_2$  in contrast to the centrosymmetric  $\gamma$ - $[\text{Mo}_8\text{O}_{26}]^{4-}$  isomer reported before (Figure 1d). In a similar way, single-crystal X-ray structure analysis revealed that  $\Delta$ -1 also crystallizes in chiral space group  $P2_12_12$  and exhibits the same molecular structure as  $\Lambda$ -1 but with opposite chiral configuration. As shown in Figure 1, the framework of  $\{\text{Mo}_{124}\text{Ce}_4\}$ ,  $\{\text{Mo}_8\}$  cluster and histidine ligands of  $\Delta$ -1a are a perfect mirror image of those of  $\Lambda$ -1a, indicating the enantiomeric nature of each other. Also, the BVS calculations for  $\Delta$ -1a gave values similar to those for  $\Lambda$ -1a (Table S1), suggesting they have the same dodecameric anionic core consisting of 24  $\text{Mo}^{\text{V}}$  and 12  $\mu_3$ -OH ions. The chirality and enantiopurity of  $\Lambda$ -1a and  $\Delta$ -1a could be unambiguously confirmed by their Flack parameters, which are close to zero.

**2** crystallizes in the same space group,  $P2_12_12$ , as  $\Lambda$ -1. There are two crystallographically independent wheels in the molecular structure of **2**, denoted as  $2\mathbf{a}_1$  and  $2\mathbf{a}_2$ , respectively (Figure 2a). Both wheels share the same elliptical nanoring  $\{\text{Mo}_{124}\text{Ce}_4\}$  as  $\Lambda$ -1a.  $2\mathbf{a}_1$  has the same composition as  $\Lambda$ -1a; however, the arrangement of six histidine ligands and the orientation of the encapsulated  $\{\text{Mo}_8\}$  cluster are different from  $\Lambda$ -1a (Figure 2b). Among the two pairs of histidine on the

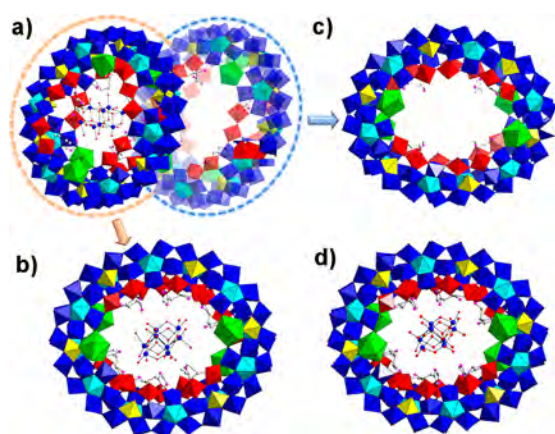


**Figure 2.** View of the molecular structures of **2a** (a), **2a<sub>1</sub>** (b), **2a<sub>2</sub>** (c), and **3a** (d). The two wheels in **2a**, namely, **2a<sub>1</sub>** and **2a<sub>2</sub>**, are highlighted with light blue and light orange circles. Color code is the same as that in Figure 1.

same side, one pair still adopts the parallel arrangement with a separation between the adjacent imidazole rings of 3.884 Å, while another pair takes a V-shaped alignment (Figure 3b). As a

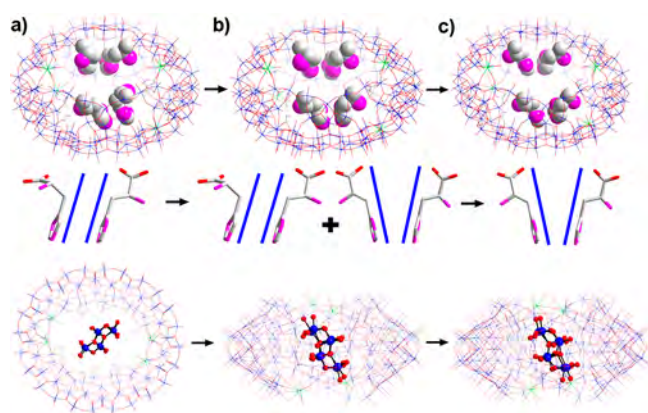


**Figure 3.** Evolution of  $\{\text{Mo}_{124}\text{Ce}_4\}$  as a confined reaction vessel that is tuned by the arrangement of L-histidine. View of the parallel arrangement of L-histidine in  $\Lambda\text{-1a}$  (a), parallel and V-shaped arrangement of L-histidine in **2a<sub>1</sub>** (b), and V-shaped arrangement of L-histidine in **3a** (c). Color code is the same as that in Figure 1.

result, the entrapped  $\{\text{Mo}_8\}$  cluster changes its orientation in relation to  $\{\text{Mo}_{124}\text{Ce}_4\}$  (Figure 3b). From the space-filling model, the  $\{\text{Mo}_8\}$  cluster is packed more tightly in the cavity of **2a<sub>1</sub>** than is the counterpart in  $\Lambda\text{-1a}$  (Figure S19). Moreover, more hydrogen bonds are found between  $\{\text{Mo}_8\}$  and histidine ligands on  $\{\text{Mo}_{124}\text{Ce}_4\}$  in **2a<sub>1</sub>**, indicating a stronger interaction between the guest and host (Figure S15). In contrast, there are only 4 histidine located on the inner surface of **2a<sub>2</sub>**. They could be divided into two sets, and each consists of two histidine attached on two  $\{\text{Mo}_2\}$  units on the same side at the most elongated points of  $\{\text{Mo}_{124}\text{Ce}_4\}$  (Figure 2c). This arrangement restrains the histidine ligands and keeps them far away from each other, generating more void space in the central cavity of **2a<sub>2</sub>**. Accordingly, no guest cluster is entrapped in the center, suggesting only  $\{\text{Mo}_8\}$ -like clusters are available, and no other clusters of the right size to be complexed in the cavity are present in solution. Notably, the absolute configuration of **2a<sub>2</sub>** ( $\Lambda$ ) is opposite that of **2a<sub>1</sub>** ( $\Delta$ ) even though the same L-histidine ligand was presented on the wheels. This means

$\{\text{Mo}_{124}\text{Ce}_4\}$  is very labile, and its absolute configuration is easily inverted in solution. On the basis of these unique structural features, **2** could be regarded as an intermediate during the self-assembly of  $\Lambda\text{-1a}$  when an inadequate amount of histidine is used in the reaction. If adequate histidine is used, then  $\Lambda\text{-1a}$  is found as the only product.

**3** crystallizes in the chiral space group  $P2_1$ . The molecular structure of **3a** is similar to those of  $\Lambda\text{-1a}$  and **2a<sub>1</sub>** (Figure 2d). The main difference lies on the different arrangement of two pairs of histidine ligands. In this case, both pairs of histidine take the V-shaped arrangement (Figure 3c). However, the entrapped  $\{\text{Mo}_8\}$  cluster still adopts the same orientation as the one in **2a<sub>1</sub>**. Similarly, multiple hydrogen bonds could be found between the protonated histidine ligands and  $\{\text{Mo}_8\}$  cluster to stabilize the whole structure (Figure S15). Having similar structural features and the same composition as those of  $\Lambda\text{-1a}$  and **3a**, **2a<sub>1</sub>** can be considered to be an isomer of  $\Lambda\text{-1a}$ .

**4** and **5** share the same framework of  $\{\text{Mo}_{124}\text{Ce}_4\}$  as **1** but with arginine and tryptophan grafted on the inner ring instead of histidine. Moreover, no POM clusters are captured within the void space of the ring. Since  $\Delta\text{-4}$  and  $\Delta\text{-5}$  are enantiomers of  $\Lambda\text{-4}$  and  $\Lambda\text{-5}$ , respectively,  $\Lambda\text{-4}$  and  $\Lambda\text{-5}$  are selected to elucidate the crystal structures.  $\Lambda\text{-4a}$  adopts the same framework as  $\Lambda\text{-1a}$  but with 6 D-tryptophan grafted on  $\{\text{Mo}_{124}\text{Ce}_4\}$ . Similar to  $\Lambda\text{-1a}$ , four of the ligands are located on one side in two pairs in parallel with a separation between pyrrole and phenyl rings of 3.570 Å, while two more are located on another side of  $\{\text{Mo}_{124}\text{Ce}_4\}$  (Figure 4a). To minimize the steric hindrance, the

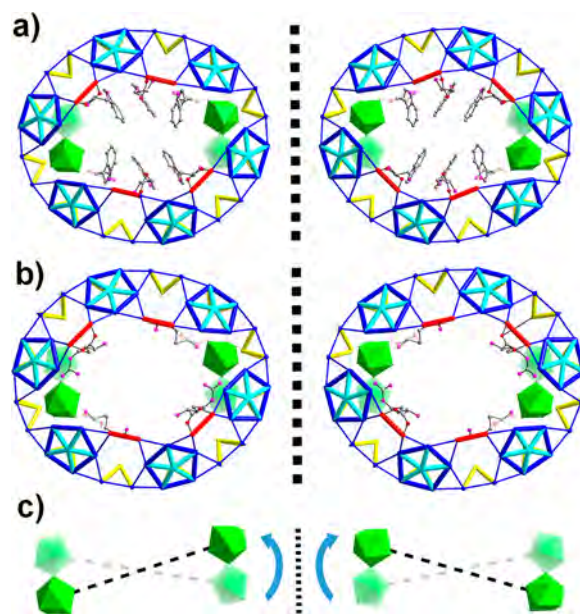


**Figure 4.** (a) View of the simplified framework of  $\Lambda\text{-4a}$  (left) and  $\Delta\text{-4a}$  (right) to highlight the basic  $\{\text{Mo}_8\}$ ,  $\{\text{Mo}_2\}$ , and  $\{\text{Mo}_1\}$  building blocks. (b) View of the simplified framework of  $\Lambda\text{-5a}$  (left) and  $\Delta\text{-5a}$  (right). (c) Representation of the absolute configurations of  $\Lambda\text{-4a}$  and  $\Lambda\text{-5a}$  (left) and  $\Delta\text{-4a}$  and  $\Delta\text{-5a}$  (right) based on the helical arrangement of  $\text{Ce}^{3+}$  ions. The  $\text{Ce}^{3+}$  ions behind the plane is highlighted in transparency.

carboxylates of the two D-tryptophan ligands in the middle adopt monodentate rather than the classic bidentate chelate coordination modes adopted by histidine (Figure S22). Interestingly, one protonated D-kynurenine other than D-tryptophan is found as counterion to balance the charge of  $\Lambda\text{-4a}$



(see discussion in the later section). It is well-known that D-kynurenine is a metabolite formed during the metabolism of D-tryptophan and that the generation of D-kynurenine is promoted by several enzymes.<sup>15</sup> In  $\Lambda$ -4, we propose that the generation of D-kynurenine may be derived from the oxidative cleavage promoted by  $\{\text{Mo}_{124}\text{Ce}_4\}$ . More discussion will be presented in section below.  $\Lambda$ -5a has the same framework as  $\Lambda$ -4a, but only 4 D-arginine are located on the inner surface, which is similar to  $2a_2$ . Due to the flexibility of the alkyl backbone, D-arginine is almost completely encapsulated within the pitch of  $\{\text{Mo}_{124}\text{Ce}_4\}$ , thus leaving an accessible pore with a dimension of  $\sim 15 \text{ \AA} \times 12 \text{ \AA}$  (Figure S17).

Although  $\{\text{Mo}_{124}\text{Ce}_4\}$  adopts the same absolute configuration in  $\Lambda$ -1a,  $\Lambda$ -4a, and  $\Lambda$ -5a, the amino acids (AA) incorporated adopt the L-configuration for  $\Lambda$ -1a and D-configuration for  $\Lambda$ -4a and  $\Lambda$ -5a. Because both  $\{\text{Mo}_{124}\text{Ce}_4\}$  and amino acids can exhibit chirality, the combination of them will, in principle, lead to four diastereomers which could be divided into two pairs of enantiomers, i.e.,  $\Delta$ - $\{\text{Mo}_{124}\text{Ce}_4\}$ -L-AA and  $\Lambda$ - $\{\text{Mo}_{124}\text{Ce}_4\}$ -D-AA,  $\Lambda$ - $\{\text{Mo}_{124}\text{Ce}_4\}$ -L-AA and  $\Delta$ - $\{\text{Mo}_{124}\text{Ce}_4\}$ -D-AA. However, only one pair of enantiomers will be produced for a certain type of amino acid due to the stereoselective synthesis, as indicated by the case of  $\Lambda$ - $\{\text{Mo}_{124}\text{Ce}_4\}$ -L-His ( $\Lambda$ -1a) and  $\Delta$ - $\{\text{Mo}_{124}\text{Ce}_4\}$ -D-His ( $\Delta$ -1a). As mentioned above,  $\{\text{Mo}_{124}\text{Ce}_4\}$  is very labile in solution. Therefore, it is possible that  $\{\text{Mo}_{124}\text{Ce}_4\}$  can adopt the same configuration when different amino acids with the opposite chirality are used, which is the case for in  $\Lambda$ -1a,  $\Lambda$ -4a, and  $\Lambda$ -5a.

Both 6 and 7 crystallize in the centrosymmetric space group  $C_2/m$  and comprise an archetypal  $\{\text{Mo}_{154}\}$  framework that is composed of 14 sets of  $\{\text{Mo}_8\}$ ,  $\{\text{Mo}_2\}$ , and  $\{\text{Mo}_1\}$  building blocks (Figure 5). In 6a, 4 histidine ligands are functionalized

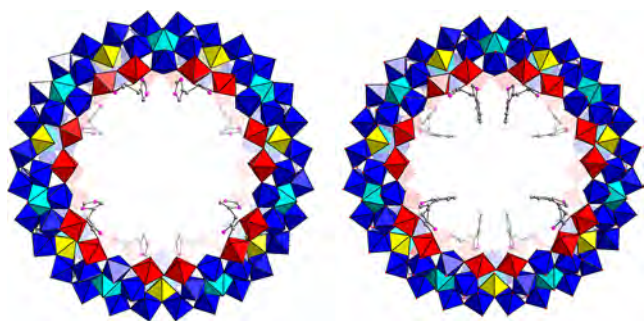


**Figure 5.** View of the molecular structure of 6a (left) and 7a (right). The 4 histidine/tryptophan ligands on the back side of  $\{\text{Mo}_{154}\}$  is highlighted in transparency. Color code is the same as that in Figure 1.

on 4  $\{\text{Mo}_2\}$  units on one side of  $\{\text{Mo}_{154}\}$ , and another side is functionalized by 4 symmetrically related histidine. Two of them align in V-shaped arrangement on two adjacent  $\{\text{Mo}_2\}$  units, while another 2 histidine are alternately attached on the other 4  $\{\text{Mo}_2\}$ . Although L-histidine is used in the synthesis, it could not be fully elucidated in the crystal structure. This is caused by the high molecular symmetry of  $\{\text{Mo}_{154}\}$  ( $D_{7d}$ ), which dominates the symmetry of 6 and thus makes the whole structure centrosymmetric instead of chiral.<sup>9</sup> This indicates that L-histidine itself could not transfer its chirality to the framework of 6a efficiently. Compound 7 has a structure similar to that of 6 but with 8 L-tryptophan ligands grafted on the inner surface, which adopt the same arrangement as L-histidine in 6.

**Important Role of  $\text{Ce}^{3+}$  Ions during Self-Assembly and Crystallization.** On the basis of the crystal structures of 1–7,

it could be clearly seen that  $\text{Ce}^{3+}$  ion is essential for the formation of chiral MB compounds 1–5. Without addition of  $\text{Ce}^{3+}$  ion as “symmetry breaker”, 6 and 7 were produced and yield a centrosymmetric  $\{\text{Mo}_{154}\}$  motif that dominates the symmetry of the whole structure. In this case, L-histidine or L-tryptophan cannot transfer chirality efficiently to  $\{\text{Mo}_{154}\}$ . Therefore, the stereoselective synthesis of chiral MB will occur only if  $\text{Ce}^{3+}$  ions are employed to trigger the formation of the racemic LMB with chiral configuration. This confirms our hypothesis in Scheme 1. It should be noted that isostructural chiral MB can be readily obtained when replacing  $\text{Ce}^{3+}$  with  $\text{Gd}^{3+}$  and  $\text{Sm}^{3+}$  in the synthesis of 1. Indeed, if only  $\text{Ce}^{3+}$  ions are introduced in the synthesis in the absence of amino acids, then racemic LMB  $\{\text{Mo}_{126}\text{Ce}_4\}$  is obtained. This compound has a molecular similar structure to that of  $\{\text{Mo}_{124}\text{Ce}_4\}$  in 1–5 and exhibits a helical chiral configuration of both  $\Delta$  and  $\Lambda$  in 1:1 ratio (Figure S21).<sup>16</sup>

**$\{\text{Mo}_{124}\text{Ce}_4\}$  as Confined Reaction Vessel and Transformation of Tryptophan to Kynurenine.** On closer inspection of the crystal structures of 1–5, all of these compounds share the same framework of  $\{\text{Mo}_{124}\text{Ce}_4\}$ . However, only 1–3 comprise the  $\{\text{Mo}_8\}@ \{\text{Mo}_{124}\text{Ce}_4\}$  moiety, while nothing is entrapped within 4 and 5. This indicates the following: (1)  $\{\text{Mo}_8\}$  is either a template that directs the self-assembly of  $\{\text{Mo}_{124}\text{Ce}_4\}$  or a guest trapped by  $\{\text{Mo}_{124}\text{Ce}_4\}$ . (2) Histidine is essential for the trapping of  $\{\text{Mo}_8\}$  in 1–3 since other amino acids such as arginine and tryptophan do not result in its formation. In addition, steric hindrance is critical for the encapsulation of  $\{\text{Mo}_8\}$  within  $\{\text{Mo}_{124}\text{Ce}_4\}$ . No POM cluster is encapsulated within  $2a_2$ , although this wheel is also functionalized by L-histidine. The main difference is that 4 histidine are attached on  $2a_2$  while 6 histidine are bound on 1,  $2a_1$ , and 3, demonstrating the importance of steric hindrance. Moreover, the orientation of  $\{\text{Mo}_8\}$  within  $\{\text{Mo}_{124}\text{Ce}_4\}$  is directly related with the spatial arrangement of L-histidine. As shown in Figure 3, when the two pairs of histidine ligands change from parallel ( $\Lambda$ -1) to combined parallel and V-shaped ( $2a_1$ ) and to V-shaped ( $3a$ ) arrangement, the entrapped  $\{\text{Mo}_8\}$  changes its orientation by rotating  $\sim 90^\circ$  around the short axis of ellipsoid-shaped  $\{\text{Mo}_{124}\text{Ce}_4\}$  accordingly. In this context, the  $\{\text{Mo}_{124}\text{Ce}_4\}$  could be regarded as a confined reaction vessel where chiral  $\{\text{Mo}_8\}$  could be generated *in situ*, and its orientation could be tuned by changing the spatial arrangement of L-histidine ligands. A similar phenomenon has already been discovered in  $\{\text{Mo}_{24}\text{Fe}_{12}\}$  macrocycle system where the ring acts as a confined reaction vessel to produce a novel  $\{\text{Mo}_{12}\text{O}_{36}(\text{HPO}_3)_2\}$  cluster.<sup>17</sup>

As mentioned above, one protonated kynurenine is detected as counterion in the crystal structure of 4 (Figure 6).

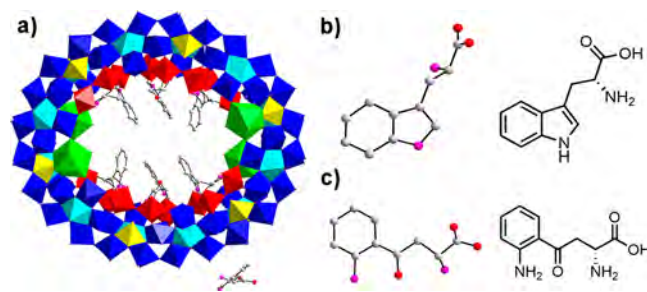


**Figure 6.** View of the molecular structure of  $\Lambda$ -4a (a); D-tryptophan (b) attached on  $\Lambda$ -4a and D-kynurenine (c) as counterion. Color code is the same as that in Figure 1.

L-Kynurenine is a key intermediate metabolite during the metabolism of L-tryptophan, and more than 95% of tryptophan is metabolized through the kynurenine pathway.<sup>15</sup> Upon entering the kynurenine pathway, tryptophan is first converted to N-formyl-L-kynurenine by tryptophan 2,3-dioxygenase (TDO) and indoleamine 2,3-dioxygenase (IDO) via oxidativative cleavage, and then N-formyl-L-kynurenine is further degraded by formamidase to L-kynurenine via hydrolysis. Therefore, two step reactions are generally required to produce L-kynurenine from L-tryptophan, involving several highly specific enzymes. In addition to the biosynthetic route, several approaches have been developed for chemical synthesis of L-kynurenine; however, most of them involve multistep synthesis and suffer from tedious purification.<sup>18</sup> In the case of **4**, the synthesis proceeds in a very straightforward manner and gives L- or D-kynurenine cleanly in a one-pot reaction (Figure 6).

As we know, POM clusters are widely used as versatile catalysts to promote a variety of chemical transformations including epoxidation, sulfoxidation, phosphoester hydrolysis, and so on.<sup>2c</sup> In particular, some POM clusters have shown good performance toward oxidativative cleavage of C–C bonds and the hydrolysis of peptides.<sup>19</sup> Moreover, {Mo<sub>154</sub>} has already been reported as an efficient catalyst for the partial oxidation of cyclohexane.<sup>20</sup> On the basis of the discussion above, we tentatively propose that the {Mo<sub>124</sub>Ce<sub>4</sub>} can act to generate kynurenine *in situ* via oxidativative cleavage and hydrolysis of tryptophan. During the self-assembly of **4**, the formation of {Mo<sub>124</sub>Ce<sub>4</sub>} is very fast, as indicated by a mechanistic study of MB cluster,<sup>21</sup> the L-tryptophan coordinated to {Mo<sub>2</sub>} units are thus encapsulated within the cavity of {Mo<sub>124</sub>Ce<sub>4</sub>} very quickly. In this way, the pyrrole rings on tryptophan ligands are well-protected in the wheels and thus avoid the discussed chemical transformation. In contrast, the tryptophan that is located externally has unconstrained access to {Mo<sub>124</sub>Ce<sub>4</sub>} and thus undergoes oxidative cleavage and subsequent hydrolysis. This finally results in the formation of **4a** with intact tryptophan anchored on inner surface and kynurenine as counterion. The proposed route of transformation of tryptophan to kynurenine is deduced based on the reported MB and other well-established POM catalysis systems; more experiments are therefore required to validate the mechanistic transformation, which is beyond the scope of current study and will be comprehensively investigated in the future. The successful production of kynurenine indicates that MB clusters have the potential to be used for selective oxidation.

**CD, <sup>1</sup>H NMR, and ESI-IMS-MS Studies.** The solution CD spectra of Δ-1 and Λ-1 are mirror images of each other, and each exhibit a characteristic exciton splitting centered at 234 and 274 nm that originated from histidine (Figure 7). Compared with the free histidine, the redshift of CD signal (~20 nm) suggests that histidine ligands are attached on {Mo<sub>124</sub>Ce<sub>4</sub>} and that the fixation of carboxylate on {Mo<sub>2</sub>} units limits the free rotation of histidine and thus reinforces the conjugated system of histidine.

However, the CD signal corresponding to {Mo<sub>124</sub>Ce<sub>4</sub>} is not detected owing to the rather strong adsorption arising from intervalence charge-transfer between Mo<sup>V</sup> and Mo<sup>VI</sup> centers which greatly suppress weak CD response induced by histidine ligands. The solution CD spectra of Δ-4 and Λ-4, as well as those of Δ-5 and Λ-5, are also mirror images of each other and exhibit profiles similar to those of the free amino acid ligands with a bit of red-shift (Figures S24 and 25). This indicates that compounds **1**, **4**, and **5** preserve their chirality in solution, in addition to the solid-state.

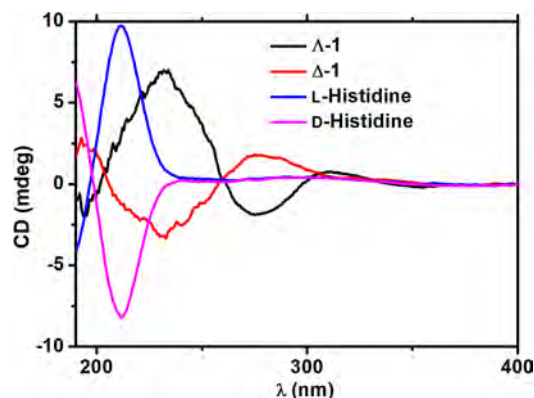


Figure 7. Solution CD spectra of Λ-1, Δ-1, L-histidine, and D-histidine.

The <sup>1</sup>H NMR spectrum of Λ-1 shows a pattern similar to that of free histidine (Figure 8). However, the related proton

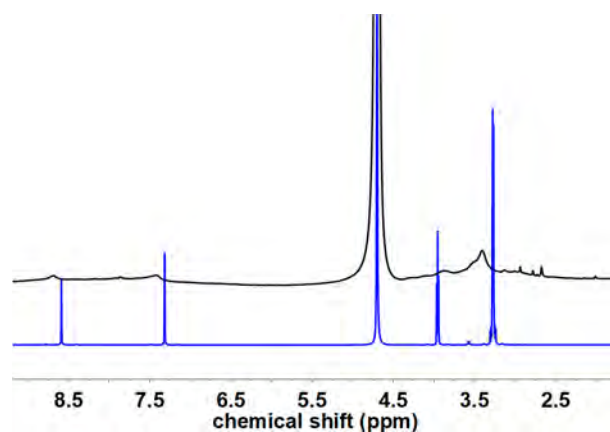


Figure 8. <sup>1</sup>H NMR spectra of Λ-1 (black, top trace) and L-histidine (blue, bottom trace).

resonances become rather broad, and both the signals from imidazole and alkyl groups display obvious upfield or downfield shifts in Λ-1a. This demonstrates the histidine ligand is confined in a paramagnetic environment, and the broadening and shift of proton signals are probably caused by the shielding effect from reduced {Mo<sub>124</sub>Ce<sub>4</sub>}.<sup>9b</sup> Attempts to obtain <sup>1</sup>H NMR spectra of Λ-4 and Λ-5 failed due to their rather poor solubility in D<sub>2</sub>O.

Due to the limited solubility, Λ-4 was decomposed by Na<sub>2</sub>H<sub>2</sub>EDTA (EDTA = ethylenediaminetetraacetic acid) to give a clear solution for <sup>1</sup>H NMR analysis. Compared with free tryptophan and kynurenine, characteristic peaks related to kynurenine could be seen very clearly in addition to the signal corresponding to tryptophan (Figure 9). This further confirmed that kynurenine was produced *in situ* during the crystal growth of Λ-4, consistent with the crystal structure analysis. In contrast, only tryptophan was observed in the solution of decomposed **7** (Figure 9), indicating that the formation of kynurenine is very selective and can only be generated in the presence of {Mo<sub>124</sub>Ce<sub>4</sub>}.

Electrospray ion mobility-mass spectrometry (ESI-IMS-MS) is useful to investigate whether the structures are present in solution,<sup>22</sup> and spectra were acquired for compounds **1** and **5**. As an example a spectrum of Δ-5 is shown here in Figure 10, and other spectra can be seen in the Supporting Information. In all cases, a dominant series of broad signals are consistent



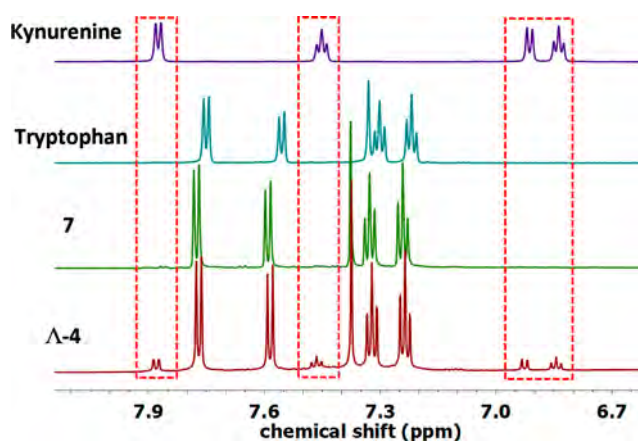


**Figure 9.**  $^1\text{H}$  NMR spectra of kynurenine, tryptophan, decomposed **7**, and decomposed  $\Delta$ -4 (from top to bottom). Inserted dashed line framework contains the signals corresponding to kynurenine.

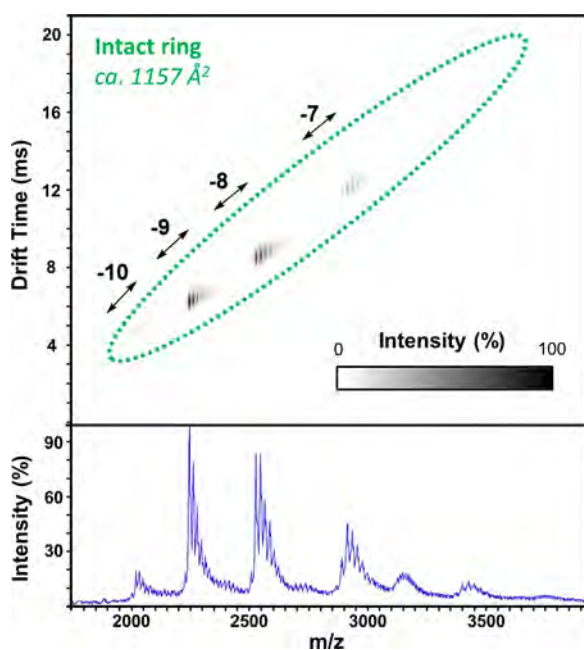


**Figure 10.** ESI-IMS-MS spectrum (above) of a solution of  $\Delta$ -5, along with standard ESI-MS spectrum (below).

with signals with the rings remaining intact in solution (ionised in a range of charge states), with a mixture of cations (these peaks are often “jagged”, corresponding to the sequential loss of small peripheral building blocks).<sup>8c,17</sup> Intact molecular species for the wheel of  $\Delta$ -5 could be detected at  $m/z$  2033.1 for  $[\text{Mo}_{124}\text{Ce}_4\text{O}_{376}(\text{H}_2\text{O})_{64}\text{H}_{10}(\text{C}_6\text{H}_{14}\text{N}_4\text{O}_2)_4]^{10-}$ , 2261.2 for  $[\text{Mo}_{124}\text{Ce}_4\text{O}_{376}(\text{H}_2\text{O})_{65}\text{H}_{11}(\text{C}_6\text{H}_{14}\text{N}_4\text{O}_2)_4]^{9-}$ , 2545.6 for  $[\text{Mo}_{124}\text{Ce}_4\text{O}_{376}(\text{H}_2\text{O})_{66}\text{H}_{12}(\text{C}_6\text{H}_{14}\text{N}_4\text{O}_2)_4]^{8-}$ , and 2928.7 for  $(\text{C}_5\text{H}_{15}\text{N}_4\text{O}_2)-[\text{Mo}_{124}\text{Ce}_4\text{O}_{376}(\text{H}_2\text{O})_{64}\text{H}_{12}(\text{C}_6\text{H}_{14}\text{N}_4\text{O}_2)_4]^{7-}$  (Table S5). Faint signals which are consistent with the dimeric aggregation of these structures (signals below green ring) were also observed in all cases, although it is not clear if this occurs in solution or upon transfer to the gas phase.

## CONCLUSIONS

In summary, we have developed a novel synthetic strategy using  $\text{Ce}^{3+}$  ions as symmetry breakers and amino acids as chiral ligands, and a series of chiral MB clusters **1–5** have been

successfully constructed which exploit the synergistic effects of combining both the lanthanide ions and amino acids in the MB synthesis. Both lanthanide ions and amino acids are essential for the synthesis, and neither  $\text{Ce}^{3+}$  ions nor amino acids themselves alone can lead to the formation of enantiopure chiral wheels but racemic LMB or centrosymmetric amino acid-functionalized MB **6** and **7**. All the chiral MB share the same chiral framework of  $\{\text{Mo}_{124}\text{Ce}_4\}$  with the inner surfaces being functionalized by histidine, tryptophan or arginine. The chiralities of **1–5** are confirmed both in solid-state and solution, as indicated by single-crystal X-ray structure analysis and CD spectroscopy, respectively. The solution behavior of these clusters was studied by  $^1\text{H}$  NMR and ESI-IMS-MS, confirming their stabilities in solution and potential availabilities for higher order assembly. Interestingly, the chirality of  $\{\text{Mo}_{124}\text{Ce}_4\}$  is very labile and could be tuned by changing different types of amino acids. Moreover, with histidine ligands, the  $\{\text{Mo}_{124}\text{Ce}_4\}$  wheel acts as a reaction vessel during the self-assembly where a  $\{\text{Mo}_8\}$  cluster is generated *in situ*, and the orientation of  $\{\text{Mo}_8\}$  cluster is controlled by the spatial arrangement of histidine ligands. In the case of tryptophan,  $\{\text{Mo}_{124}\text{Ce}_4\}$  promotes the transformation of tryptophan to kynurenine with high selectivity. In future, we will continue to explore the potential use of these wheels for chiral recognition and asymmetric catalysis based on their inherent chirality and porosity.

## EXPERIMENTAL METHODS

**Materials and Instrumentations.** All reagents and solvents were purchased from commercial sources and used as received. Elemental analyses (Mo, Ce, and Na) were performed via ICP-OES. C, H, and N contents were determined by the microanalysis using an EA 1110 CHNS, CE-440 Elemental Analyzer. Thermogravimetric analysis was performed on a TA Instruments Q 500 Thermogravimetric Analyzer under nitrogen flow at a typical heating rate of  $10\text{ }^\circ\text{C min}^{-1}$ . UV–vis–NIR spectra were collected using a Shimadzu PharmaSpec UV-1700 UV–vis spectrophotometer in transmission mode using quartz cuvettes with 1.0 cm optical path length. Infrared spectra ( $4000\text{--}400\text{ cm}^{-1}$ ) of all samples were recorded on JASCO FTIR-410 spectrometer or a JASCO FT-IR 4100 spectrometer. CD spectra were collected on a J-710 spectropolarimeter (Jasco, Japan).  $^1\text{H}$  NMR spectra were recorded on a Bruker DPX 500 spectrometer. ESI-ion mobility mass spectra were acquired on a Waters Synapt G2 HDMS instrument.

**X-ray Crystal Structure Analyses.** Suitable single crystals were selected and mounted onto a rubber loop using Fomblin oil. Single crystal X-ray diffraction data of **1**, **2**, and **4–7** were recorded on a Bruker Apex CCD diffractometer ( $\lambda(\text{Mo K}\alpha) = 0.71073\text{ \AA}$ ) at 150 K equipped with a microfocus X-ray source (50 kV, 30w). The data of compound **3** was collected on Beamline I19 at the UK Diamond Light Source ( $\lambda = 0.6889\text{ \AA}$ ) at 100 K. Data collection and reduction were performed using the Apex3 or CrysAlisPro software package and structure solution, and refinement was carried out by SHELXS-2014 and SHELXL-2014 using WinGX.<sup>10</sup> Corrections for incident and diffracted beam absorption effects were applied using empirical absorption correction. All the Mo atoms (including those disordered), Ce atoms, and most of the O atoms were refined anisotropically. Sodium ions were identified and refined isotropically. Solvent water molecule sites with partial occupancy were found and included in the structure refinement. Crystallographic formulas typically contain many more water molecules in the crystal lattice than those found in the sample after drying. With these structures, we are moving outside the realm of small-molecule crystallography, dealing with refinements and problems that lie between small-molecule and protein crystallography. As a result, the refinement statistics are similar to those found for protein structures. However, the final refinement statistics are relatively good, and in all cases, the structural analysis allows us to unambiguously determine the structures of the compounds. All the

structures of compounds 1–7 were deposited at Cambridge Crystallographic Data Center; the data can be obtained via [www.ccdc.cam.ac.uk/data\\_request/cif](http://www.ccdc.cam.ac.uk/data_request/cif) under deposition numbers CCDC 1853666–1853671 and 853695–1853698.

**Synthesis of  $\Lambda$ -1.**  $\text{CeCl}_3 \cdot 7\text{H}_2\text{O}$  (37.5 mg, 0.1 mmol), L-histidine (7.7 mg, 0.05 mmol), and an aqueous solution of 0.1 M  $[\text{N}_2\text{H}_4] \cdot 2\text{HCl}$  (0.4 mL) were added to a solution of  $\text{Na}_2\text{MoO}_4 \cdot 2\text{H}_2\text{O}$  (242 mg, 1 mmol) in water (40 mL) and 1 M  $\text{HClO}_4$  (4.5 mL). The mixture was then heated with medium stirring in a 100 mL Erlenmeyer flask (wide-necked; covered with a watch glass) at 90 °C for 1 h. The resulting clear deep-blue solution was then cooled to room temperature, filtered, and kept in an open 100 mL Erlenmeyer flask for 1 week. The deep-blue blocklike crystals were collected by filtration, washed with ice-cold  $\text{H}_2\text{O}$ , and dried under inert atmosphere over  $\text{CaCl}_2$ . Yield: 71 mg (35.1% based on Mo). Elemental analysis, calcd: C, 2.30%; H, 2.20%; N, 1.34%; Na, 0%; Mo, 50.70%; Ce, 2.24%. Found: C, 2.48%; H, 1.09%; N, 1.23%; Na, 0.026%; Mo, 49.13%; Ce, 2.33%. IR (KBr pellet, 4000–600  $\text{cm}^{-1}$ ): 3384(s, br), 3145(s, br), 2927(w), 2857(w), 1726(w), 1617(s), 1502(w), 1430(w), 973(s), 907(w), 866(m), 803(sh), 708(m), 674(m), 645(m).

**Synthesis of  $\Delta$ -1.** The synthetic procedure is the same as that for  $\Lambda$ -1 but uses D-histidine (7.7 mg, 0.05 mmol). Yield: 75 mg (37.6% based on Mo). Elemental analysis, calcd: C, 2.30%; H, 2.20%; N, 1.34%; Na, 0%; Mo, 50.70%; Ce, 2.24%. Found: C, 2.49%; H, 1.09%; N, 1.45%; Na, 0.053%; Mo, 50.7%; Ce, 2.49%. IR (KBr pellet, 4000–600  $\text{cm}^{-1}$ ): 3365(s, br), 3147(s, br), 2925(w), 2854(w), 1738(2), 1617(s), 1493(w, br), 1427(w), 976(s), 909(w), 875(m), 809(sh), 744(m), 677(m), 642(m).

**Synthesis of 2.**  $\text{CeCl}_3 \cdot 7\text{H}_2\text{O}$  (30.0 mg, 0.08 mmol), L-histidine (6.2 mg, 0.04 mmol), and an aqueous solution of 0.1 M  $[\text{N}_2\text{H}_4] \cdot 2\text{HCl}$  (0.4 mL) were added to a solution of  $\text{Na}_2\text{MoO}_4 \cdot 2\text{H}_2\text{O}$  (242 mg, 1 mmol) in water (45 mL) and 1 M  $\text{HClO}_4$  (4.5 mL). The mixture was then heated with medium stirring in a 100 mL Erlenmeyer flask (wide-necked; covered with a watch glass) at 90 °C for 1 h. The resulting clear deep-blue solution was then cooled to room temperature, filtered, and kept in an open 100 mL Erlenmeyer flask for 3 weeks. The deep-blue blocklike crystals were collected by filtration, washed with ice-cold  $\text{H}_2\text{O}$ , and dried under inert atmosphere over  $\text{CaCl}_2$ . Yield: 71 mg (35.1% based on Mo). Elemental analysis, calcd: C, 2.07%; H, 2.25%; N, 1.20%; Na, 0.28%; Mo, 50.29%; Ce, 2.30%. Found: C, 1.97%; H, 1.77%; N, 1.11%; Na, 0.28%; Mo, 51.01%; Ce, 2.47%. IR (KBr pellet, 4000–600  $\text{cm}^{-1}$ ): 3372(s, br), 3132(s, br), 2921(w), 2861(w), 1607(s), 1491(w, br), 1433(w), 1346(w), 1296(w), 1247(w), 1147(w), 1094(w, br), 973(s), 905(w), 869(m), 803(m), 740(m), 637(s), 554(s).

**Synthesis of 3.**  $\text{CeCl}_3 \cdot 7\text{H}_2\text{O}$  (150 mg, 0.4 mmol), L-histidine (18.6 mg, 0.12 mmol), and an aqueous solution of 0.1 M  $[\text{N}_2\text{H}_4] \cdot 2\text{HCl}$  (1.6 mL) were added to a solution of  $\text{Na}_2\text{MoO}_4 \cdot 2\text{H}_2\text{O}$  (1.0 g, 4.2 mmol) in water (130 mL). Then, pH was adjusted to 1.2–1.3 by 70%  $\text{HClO}_4$ . Afterward, the mixture was heated with medium stirring in a 250 mL Erlenmeyer flask (wide-necked; covered with a watch glass) at 90 °C for 1 h. The resulting clear deep-blue solution was then cooled to room temperature, filtered, and kept in an open 250 mL Erlenmeyer flask for 5 weeks. The deep-blue blocklike crystals were collected by filtration, washed with ice-cold  $\text{H}_2\text{O}$ , and dried under inert atmosphere over  $\text{CaCl}_2$ . Yield: 30 mg (40.1% based on Mo). Elemental analysis, calcd: C, 1.77%; H, 2.10%; N, 1.03%; Na, 0%; Mo, 51.72%; Ce, 2.29%. Found: C, 1.80%; H, 1.71%; Na, 1.01%; Mo, 0.046%; Mo, 50.78%; Ce, 1.95%. IR (KBr pellet, 4000–600  $\text{cm}^{-1}$ ): 3386(s, br), 3144(s, br), 2920(w), 2853(w), 1609(s), 1490(w, br), 1419(w), 1337(w), 1241(w), 1087(w, br), 990(m), 969(s), 904(w), 860(m), 740(m), 709(w), 675(m).

**Synthesis of  $\Delta$ -4.**  $\text{CeCl}_3 \cdot 7\text{H}_2\text{O}$  (37.5 mg, 0.1 mmol), L-tryptophan (29 mg, 0.14 mmol), and an aqueous solution of 0.1 M  $[\text{N}_2\text{H}_4] \cdot 2\text{HCl}$  (0.4 mL) were added to a solution of  $\text{Na}_2\text{MoO}_4 \cdot 2\text{H}_2\text{O}$  (242 mg, 1 mmol) in water (40 mL) and 1 M  $\text{HClO}_4$  (4.5 mL). The mixture was then heated with medium stirring in a 100 mL Erlenmeyer flask (wide-necked; covered with a watch glass) at 90 °C for 1 h. The resulting clear deep-blue solution was then cooled to room temperature, filtered, and kept in an open 100 mL Erlenmeyer flask for 5 weeks. The deep-blue

blocklike crystals were collected by filtration, washed with ice-cold  $\text{H}_2\text{O}$ , and dried under inert atmosphere over  $\text{CaCl}_2$ . Yield: 30 mg (15.8% based on Mo). Elemental analysis, calcd: C, 4.31%; H, 2.25%; N, 0.94%; Na, 0.19%; Mo, 49.65%; Ce, 2.34%. Found: C, 4.88%; H, 1.44%; N, 1.09%; Na, 0.17%; Mo, 49.80%; Ce, 1.95%. IR (KBr pellet, 4000–600  $\text{cm}^{-1}$ ): 3396(s, br), 3164(s, br), 2925(w), 2857(w), 1607(s), 1494(w, br), 1423(w), 1340(w), 1247(w), 1094(w, br), 991(m), 973(s), 905(w), 865(m), 741(m), 711(w), 677(m).

**Synthesis of  $\Lambda$ -4.** The synthetic procedure is the same as that for  $\Delta$ -4 but uses D-tryptophan (29 mg, 0.14 mmol). Yield: 32 mg (16.6% based on Mo). Elemental analysis, calcd: C, 4.31%; H, 2.25%; N, 0.94%; Na, 0.19%; Mo, 49.65%; Ce, 2.34%. Found: C, 4.76%; H, 1.57%; N, 1.09%; Na, 0.22%; Mo, 50.10%; Ce, 2.13%. IR (KBr pellet, 4000–600  $\text{cm}^{-1}$ ): 3376(s, br), 3169(s, br), 2925(w), 2857(w), 1612(s), 1491(w, br), 1340(w), 1245(w), 965(s), 902(w), 865(m), 797(w), 739(m), 704(w), 663(m).

**Synthesis of  $\Delta$ -5.**  $\text{CeCl}_3 \cdot 7\text{H}_2\text{O}$  (37.5 mg, 0.1 mmol), L-arginine (7.0 mg, 0.04 mmol), and an aqueous solution of 0.1 M  $[\text{N}_2\text{H}_4] \cdot 2\text{HCl}$  (0.4 mL) were added to a solution of  $\text{Na}_2\text{MoO}_4 \cdot 2\text{H}_2\text{O}$  (242 mg, 1 mmol) in water (40 mL) and 1 M  $\text{HClO}_4$  (4.5 mL). The mixture was then heated with medium stirring in a 100 mL Erlenmeyer flask (wide-necked; covered with a watch glass) at 90 °C for 1 h. The resulting clear deep-blue solution was then cooled to room temperature, filtered, and kept in an open 100 mL Erlenmeyer flask for 1 week. The deep-blue blocklike crystals were collected by filtration, washed with ice-cold  $\text{H}_2\text{O}$ , and dried under inert atmosphere over  $\text{CaCl}_2$ . Yield: 90 mg (48.7% based on Mo). Elemental analysis, calcd: C, 1.83%; H, 2.36%; N, 1.43%; Na, 0%; Mo, 50.46%; Ce, 2.38%. Found: C, 1.89%; H, 1.37%; N, 1.43%; Na, 0.050%; Mo, 50.00%; Ce, 2.38%. IR (KBr pellet, 4000–600  $\text{cm}^{-1}$ ): 3352(s, br), 3183(s, br), 2927(w), 2854(w), 1611(s), 1505(w), 1430(w), 1349(w), 964(s), 898(w), 839(m), 803(m), 744(m).

**Synthesis of  $\Lambda$ -5.** The synthetic procedure is the same as that for  $\Delta$ -5 but uses D-arginine (7.0 mg, 0.04 mmol). Yield: 86 mg (45.5% based on Mo). Elemental analysis, calcd: C, 1.83%; H, 2.36%; N, 1.43%; Na, 0%; Mo, 50.46%; Ce, 2.38%. Found: C, 1.91%; H, 1.58%; N, 1.43%; Na, 0.055%; Mo, 50.10%; Ce, 2.38%. IR (KBr pellet, 4000–600  $\text{cm}^{-1}$ ): 3355(s, br), 3173(s, br), 2927(w), 2854(w), 1615(s), 1502(w), 1427(w), 1356(w), 970(s), 901(w), 843(m), 800(m), 746(m).

**Synthesis of 6.** L-Histidine (10 mg, 0.065 mmol) and an aqueous solution of 0.1 M  $[\text{N}_2\text{H}_4] \cdot 2\text{HCl}$  (0.4 mL) were added to a solution of  $\text{Na}_2\text{MoO}_4 \cdot 2\text{H}_2\text{O}$  (242 mg, 1 mmol) in water (45 mL) and 1 M  $\text{HClO}_4$  (4.5 mL). The mixture was then heated with medium stirring in a 100 mL Erlenmeyer flask (wide-necked; covered with a watch glass) at 90 °C for 1 h. The resulting clear deep-blue solution was then cooled to room temperature, filtered, and kept in an open 100 mL Erlenmeyer flask for 2 weeks. The deep-blue blocklike crystals were collected by filtration, washed with ice-cold  $\text{H}_2\text{O}$ , and dried under inert atmosphere over  $\text{CaCl}_2$ . Yield: 50 mg (27.4% based on Mo). Elemental analysis, calcd: C, 2.05%; H, 2.17%; N, 1.20%; Na, 0.33%; Mo, 52.58%. Found: C, 2.07%; H, 1.23%; N, 1.26%; Na, 0.285%; Mo, 52.30%. IR (KBr pellet, 4000–600  $\text{cm}^{-1}$ ): 3384(s, br), 3152(s, br), 2927(w), 2854(w), 1615(s), 1494(w, br), 1247(w), 1094(w, br), 993(w), 968(s), 902(w), 870(m), 817(m), 754(m), 663(m), 646(m), 618(m).

**Synthesis of 7.** L-Tryptophan (13.3 mg, 0.065 mmol) and an aqueous solution of 0.1 M  $[\text{N}_2\text{H}_4] \cdot 2\text{HCl}$  (0.4 mL) were added to a solution of  $\text{Na}_2\text{MoO}_4 \cdot 2\text{H}_2\text{O}$  (242 mg, 1 mmol) in water (45 mL) and 1 M  $\text{HClO}_4$  (4.5 mL). The mixture was then heated with medium stirring in a 100 mL Erlenmeyer flask (wide-necked; covered with a watch glass) at 90 °C for 1 h. The resulting clear deep-blue solution was then cooled to room temperature, filtered, and kept in an open 100 mL Erlenmeyer flask for 3 weeks. The deep-blue blocklike crystals were collected by filtration, washed with ice-cold  $\text{H}_2\text{O}$ , and dried under inert atmosphere over  $\text{CaCl}_2$ . Yield: 37 mg (20.3% based on Mo). Elemental analysis, calcd: C, 4.61%; H, 2.14%; N, 0.98%; Na, 0.64%; Mo, 51.61%. Found: C, 4.46%; H, 1.97%; N, 1.07%; Na, 0.70%; Mo, 51.48%. IR (KBr pellet, 4000–600  $\text{cm}^{-1}$ ): 3396(s, br), 3164(s, br), 2925(w), 2856(w), 1607(s), 1494(w), 1423(w),



1340(w), 1247(w), 1094(w, br), 991(w), 973(s), 905(w), 865(m), 741(m), 673(m).

## ■ ASSOCIATED CONTENT

### Supporting Information

The Supporting Information is available free of charge on the ACS Publications website at DOI: 10.1021/jacs.8b09750.

Detailed synthetic procedures, crystallography, NMR spectroscopy, mass spectrometry, CD spectra (PDF)  
Crystallographic information files (ZIP)

## ■ AUTHOR INFORMATION

### Corresponding Author

\*lee.cronin@glasgow.ac.uk

### ORCID

De-Liang Long: 0000-0003-3241-2379

Leroy Cronin: 0000-0001-8035-5757

### Notes

The authors declare no competing financial interest.

## ■ ACKNOWLEDGMENTS

This work was supported by the EPSRC grants (No. EP/J015156/1; EP/L023652/1; EP/I033459/1; EP/J015156/1; EP/K023004/1; EP/L023652/1), EC grant 318671 MICRE-AGENTS, LC thanks the Royal Society/Wolfson Foundation for a Merit Award and the ERC for an Advanced Grant (ERC-ADG, 670467 SMART-POM). We thank the Diamond Light Source for time on Beamline I19 under the proposal MT16085.

## ■ REFERENCES

- (1) (a) Special Issue on Polyoxometalates. *Chem. Rev.* **1998**, *98*, 1–390. (b) Pope, M. T.; Müller, A. *Polyoxometalate Chemistry: From Topology via Self-Assembly to Applications*; Kluwer, Dordrecht, 2001. (c) Themed issue: polyoxometalate cluster science. *Chem. Soc. Rev.* **2012**, *41*, 7325–7648.
- (2) (a) Long, D.-L.; Burkholder, E.; Cronin, L. *Chem. Soc. Rev.* **2007**, *36*, 105–121. (b) Long, D.-L.; Tsunashima, R.; Cronin, L. *Angew. Chem., Int. Ed.* **2010**, *49*, 1736–1758. (c) Wang, S.-S.; Yang, G.-Y. *Chem. Rev.* **2015**, *115*, 4893–4962.
- (3) (a) Kamata, K.; Yonehara, K.; Sumida, Y.; Yamaguchi, K.; Hikichi, S.; Mizuno, N. *Science* **2003**, *300*, 964–966. (b) Rausch, B.; Symes, M. D.; Chisholm, G.; Cronin, L. *Science* **2014**, *345*, 1326–1330. (c) Busche, C.; Vilà-Nadal, L.; Yan, J.; Miras, H. N.; Long, D.-L.; Georgiev, V. P.; Asenov, A.; Pedersen, R. H.; Gadegaard, N.; Mirza, M. M.; Paul, D. J.; Poblet, J. M.; Cronin, L. *Nature* **2014**, *515*, 545–549. (d) Shiddiq, M.; Komijani, D.; Duan, Y.; Gaita-Ariño, A.; Coronado, E.; Hill, S. *Nature* **2016**, *531*, 348–351. (e) Gao, N.; Sun, H.; Dong, K.; Ren, J.; Duan, T.; Xu, C.; Qu, X. *Nat. Commun.* **2014**, *5*, 3422.
- (4) (a) Du, D.-Y.; Yan, L.-K.; Su, Z.-M.; Li, S.-L.; Lan, Y.-Q.; Wang, E.-B. *Coord. Chem. Rev.* **2013**, *257*, 702–717. (b) Hasenknopf, B.; Micoine, K.; Lacôte, E.; Thorimbert, S.; Malacria, M.; Thouvenot, R. *Eur. J. Inorg. Chem.* **2008**, *2008*, 5001–5013. (c) Han, Q.; He, C.; Zhao, M.; Qi, B.; Niu, J.; Duan, C. *J. Am. Chem. Soc.* **2013**, *135*, 10186–10189. (d) Yin, P.; Zhang, Z.-M.; Lv, H.; Li, T.; Haso, F.; Hu, L.; Zhang, B.; Bacsa, J.; Wei, Y.; Gao, Y.; Hou, Y.; Li, Y.-G.; Hill, C. L.; Wang, E.-B.; Liu, T. *Nat. Commun.* **2015**, *6*, 6475.
- (5) (a) Fang, X.; Anderson, T. M.; Hill, C. L. *Angew. Chem., Int. Ed.* **2005**, *44*, 3540–3544. (b) An, H.-Y.; Wang, E.-B.; Xiao, D.-R.; Li, Y.-G.; Su, Z.-M.; Xu, L. *Angew. Chem., Int. Ed.* **2006**, *45*, 904–908. (c) Tan, H.; Li, Y.; Zhang, Z.; Qin, C.; Wang, X.; Wang, E.; Su, Z. J. *Am. Chem. Soc.* **2007**, *129*, 10066–10067. (d) Xiao, F.; Hao, J.; Zhang, J.; Lv, C.; Yin, P.; Wang, L.; Wei, Y. *J. Am. Chem. Soc.* **2010**, *132*, 5956–5957. (e) Zang, H.; Miras, H. N.; Yan, J.; Long, D.-L.; Cronin, L. *J. Am. Chem. Soc.* **2012**, *134*, 11376–11379.
- (6) (a) Special Issue on Metalloproteins: *Nature*. **2009**, *460*, 813–862. (b) Theil, E. C. *Annu. Rev. Biochem.* **1987**, *56*, 289–315. (c) Conlan, B. F.; Gillon, A. D.; Craik, D. J.; Anderson, M. A. *Biopolymers* **2010**, *94*, 573–583.
- (7) (a) Müller, A.; Serain, C. *Acc. Chem. Res.* **2000**, *33*, 2–10. (b) Müller, A.; Gouzerh, P. *Chem. Soc. Rev.* **2012**, *41*, 7431–7463. (c) Müller, A.; Krickemeyer, E.; Meyer, J.; Bögge, H.; Peters, F.; Plass, W.; Diemann, E.; Dillinger, S.; Nonnenbruch, F.; Randerath, M.; Menke, C. *Angew. Chem., Int. Ed. Engl.* **1995**, *34*, 2122–2123. (d) Müller, A.; Krickemeyer, E.; Bögge, H.; Schmidtman, M.; Beugholt, C.; Kögerler, P.; Lu, C. *Angew. Chem., Int. Ed.* **1998**, *37*, 1220–1223. (e) Müller, A.; Beckmann, E.; Bögge, H.; Schmidtman, M.; Dress, A. *Angew. Chem., Int. Ed.* **2002**, *41*, 1162–1166.
- (8) (a) Cronin, L.; Beugholt, C.; Krickemeyer, E.; Schmidtman, M.; Bögge, H.; Kögerler, P.; Luong, T. K. K.; Müller, A. *Angew. Chem., Int. Ed.* **2002**, *41*, 2805–2808. (b) Müller, A.; Beugholt, C.; Bögge, H.; Schmidtman, M. *Inorg. Chem.* **2000**, *39*, 3112–3113. (c) Xuan, W.; Surman, A. J.; Miras, H. N.; Long, D.-L.; Cronin, L. *J. Am. Chem. Soc.* **2014**, *136*, 14114–14120. (d) Yamase, T.; Ishikawa, E.; Abe, Y.; Yano, Y. *J. Alloys Compd.* **2006**, *408–412*, 693–700.
- (9) (a) Müller, A.; Das, S. K.; Kuhlmann, C.; Bögge, H.; Schmidtman, M.; Diemann, E.; Krickemeyer, E.; Hormes, J.; Modrow, H.; Schindler, M. *Chem. Commun.* **2001**, 655–656. (b) Zhang, L.; Li, Y.; Zhou, Y. *J. Mol. Struct.* **2010**, *969*, 69–74.
- (10) (a) Sheldrick, G. M. SHELXTL, version 2014/7. <http://shelx.uni-ac.gwdg.de/SHELX/index.php>. (b) Farrugia, L. *J. Appl. Crystallogr.* **1999**, *32*, 837–838.
- (11) Müller, A.; Krickemeyer, E.; Bögge, H.; Schmidtman, M.; Beugholt, C.; Das, S. K.; Peters, F. *Chem. - Eur. J.* **1999**, *5*, 1496–1502.
- (12) Brown, I. D. In *Structure and Bonding in Crystals*; O’Keeffe, M., Navrotsky, A., Eds.; Academic Press: New York, 1981, Vol. II, 1–3013.
- (13) Jensen, K. A. *Inorg. Chem.* **1970**, *9*, 1–5.
- (14) Niven, M. L.; Cruywagen, J. J.; Heyns, J. B. B. *J. Chem. Soc., Dalton Trans.* **1991**, *8*, 2007–2011.
- (15) (a) Vécsei, L.; Szalárdy, L.; Fülöp, F.; Toldi, J. *Nat. Rev. Drug Discovery* **2013**, *12*, 64–82. (b) Wang, Y.; Liu, H.; McKenzie, G.; Witting, P. K.; Stasch, J.-P.; Hahn, M.; Changsirivathanathamrong, D.; Wu, B. J.; Ball, H. J.; Thomas, S. R.; et al. *Nat. Med.* **2010**, *16*, 279–285. (c) Bryleva, E. Y.; Brundin, L. *Neuropharmacology* **2017**, *112*, 324–330. (d) Cervenka, I.; Agudelo, L. Z.; Ruas, J. L. *Science* **2017**, *357*, eaaf9794.
- (16) The crystal structure of {Mo<sub>126</sub>Ce<sub>4</sub>} can be ambiguously determined from single crystal X-ray diffraction. See Figure S21 for details.
- (17) Xuan, W.; Surman, A. J.; Zheng, Q.; Long, D.-L.; Cronin, L. *Angew. Chem., Int. Ed.* **2016**, *55*, 12703–12707.
- (18) (a) Salituro, F. G.; McDonald, I. A. *J. Org. Chem.* **1988**, *53*, 6138–6139. (b) Hamdy, M. S.; Scott, E. L.; Carr, R. H.; Sanders, J. P. M. *Catal. Lett.* **2012**, *142*, 338–344. (c) Coste, A.; Karthikeyan, G.; Couty, F.; Evano, G. *Synthesis* **2009**, *2009*, 2927–2934. (d) Kleijn, L. H. J.; Muskens, F. M.; Oppedijk, S. F.; de Bruin, G.; Martin, N. I. *Tetrahedron Lett.* **2012**, *53*, 6430–6432.
- (19) (a) Absillis, G.; Parac-Vogt, T. N. *Inorg. Chem.* **2012**, *51*, 9902–9910. (b) Ly, H. G. T.; Absillis, G.; Janssens, R.; Proost, P.; Parac-Vogt, T. N. *Angew. Chem., Int. Ed.* **2015**, *54*, 7391–7394. (c) Sarma, B. B.; Neumann, R. *Nat. Commun.* **2014**, *5*, 4621. (d) Khenkin, A. M.; Neumann, R. *J. Am. Chem. Soc.* **2008**, *130*, 14474–14476.
- (20) (a) Liu, X.; Conte, M.; Weng, W.; He, Q.; Jenkins, R. L.; Watanabe, M.; Morgan, D. J.; Knight, D. W.; Murphy, D. M.; Whiston, K.; Kiely, C. J.; Hutchings, G. J. *Catal. Sci. Technol.* **2015**, *5*, 217–227. (b) Conte, M.; Liu, X.; Murphy, D. M.; Taylor, S. H.; Whiston, K.; Hutchings, G. J. *Catal. Lett.* **2016**, *146*, 126–135.
- (21) (a) Miras, H. N.; Cooper, G. J. T.; Long, D.-L.; Bögge, H.; Müller, A.; Streb, C.; Cronin, L. *Science* **2010**, *327*, 72–74. (b) Miras, H. N.; Richmond, C. J.; Long, D.-L.; Cronin, L. *J. Am. Chem. Soc.* **2012**, *134*, 3816–3824.
- (22) Surman, A. J.; Robbins, P. J.; Ujma, J.; Zheng, Q.; Barran, P. E.; Cronin, L. *J. Am. Chem. Soc.* **2016**, *138*, 3824–3830.